# Hypergraph representation of multilayer brain network enhances autism spectrum disorder detection

Cite as: Chaos 35, 071104 (2025); doi: 10.1063/5.0279835

Submitted: 8 May 2025 · Accepted: 25 June 2025 ·

Published Online: 15 July 2025















**AFFILIATIONS** 

### **ABSTRACT**

We present a hypergraph-based framework for analyzing functional brain networks in children with autism spectrum disorder (ASD) using resting-state electroencephalography data. Moving beyond conventional multilayer network approaches, our method captures previously undetectable higher-order connectivity patterns through a two-stage analysis: (1) constructing multilayer networks via recurrence quantification analysis to model within- and cross-frequency interactions and (2) transforming these networks into hypergraphs to better represent complex neural relationships. Our results identify distinctive connectivity signatures in ASD, particularly in bilateral frontal regions, with hypergraph representations revealing patterns obscured in traditional analyses. Most significantly, hypergraph-derived features achieved 81% classification accuracy (F1-score) using support vector machines, outperforming 57% achieved with multilayer network features. These findings demonstrate how hypergraphs can provide more stable and informative biomarkers for ASD, offering both a powerful analytical framework for studying neurodevelopmental disorders and a promising pathway toward more objective diagnostic tools. The improvement in classification performance underscores the clinical potential of this approach.

Published under an exclusive license by AIP Publishing. https://doi.org/10.1063/5.0279835

Autism spectrum disorder (ASD) is a complex neurodevelopmental condition that affects communication, behavior, and social interaction. Diagnosing ASD often relies on behavioral observations, which can be subjective and delayed. Using resting-state electroencephalography (EEG) recordings, we developed a special type of network model called a hypergraph that better captures complex brain interactions compared to traditional methods. By transforming traditional multilayer brain networks into hypergraphs, we uncovered higher-order connectivity signatures that distinguish children with ASD from typically developing peers with 81% accuracy—a significant leap over conventional methods. The findings highlight disrupted connectivity in frontal brain regions and demonstrate how advanced mathematical models can reveal hidden neural patterns, offering a promising pathway toward more objective and early diagnostic tools for ASD. This work bridges complex network theory and clinical practice, demonstrating how advanced mathematics can solve real-world medical challenges. This work represents an important step toward developing objective tools for autism diagnosis and understanding.

#### I. INTRODUCTION

Magneto- and electroencephalography (M/EEG) recordings capture complex brain activity that is fundamentally composed of a superposition of neuronal oscillations across a broad range of frequencies, often referred to as brain rhythms. These distinct rhythms are not merely passive background noise; rather, they are believed to be the electrophysiological underpinnings of functionally specialized brain activity. Particularly, slow theta oscillations (4-8 Hz) are implicated in facilitating large-scale neuronal interactions essential for human memory formation and sensorimotor integration.<sup>1,2</sup> In contrast, brain-wide alpha (8-12 Hz) and beta

<sup>&</sup>lt;sup>1</sup>Baltic Center for Neurotechnology and Artificial Intelligence, Immanuel Kant Baltic Federal University, Kaliningrad, Russia

<sup>&</sup>lt;sup>2</sup>Coordinating Center for Fundamental Research, National Medical Research Center for Therapy and Preventive Medicine,

Institute of Higher Nervous Activity and Neurophysiology of the Russian Academy of Science, Moscow, Russia

<sup>&</sup>lt;sup>4</sup>Tactile Communication Research Laboratory, Pushkin State Russian Language Institute, Moscow, Russia

a) Author to whom correspondence should be addressed: hramovae@gmail.com

(15–30 Hz) oscillations are believed to underpin top-down communication processes, sensory processing, and the mechanisms involved in perceptual decision-making.<sup>3,4</sup>

Furthermore, the interaction between neuronal oscillations across different frequency bands, a phenomenon known as crossfrequency coupling (CFC), plays a critical role in establishing precise spike-timing relationships.<sup>5</sup> This coordinated activity across frequencies facilitates the dynamic organization of neuronal ensembles that are synchronized within their respective frequency bands.<sup>6</sup> Specifically, CFC enables the temporal coordination of neural firing, allowing for communication and information transfer between neuronal populations operating at different oscillatory frequencies.<sup>7</sup> This intricate interplay of oscillations and CFC is thought to be a fundamental mechanism for integrating information across various spatial and temporal scales within the brain and, thus, is essential for complex cognitive processes.<sup>8,9</sup> So, the phase of slower oscillations might modulate the amplitude or power of faster oscillations, allowing for nested hierarchies of neural activity that support flexible and adaptive behavior. For example, gamma (30-90 Hz) oscillations are associated with local processing, while theta oscillations are thought to play a role in long-range communication, and interactions between these rhythms are implicated in cognitive processes, such as attention and working memory.5

Thus, the interaction between these various brain rhythms is crucial for the integrative capacity of the brain, allowing for seamless coordination of distributed neural processes and forming the basis of higher-order cognitive functions. 10,11 It should be noted that both within-frequency synchronization and cross-frequency coupling are crucial mechanisms for coordinating neuronal processing, enabling complex brain functions. To understand these processes from an integrative perspective, contemporary neuroscience increasingly utilizes complex network theory,<sup>12</sup> which offers a powerful set of graph-theoretical tools for characterizing brain activity, both during task performance and in the resting state. 13-15 In this context, a multilayer network model provides a particularly suitable construct for representing neuronal communication.<sup>16</sup>, Within such a model, each layer corresponds to a network of neurons synchronized within a specific frequency band, while multiplex connections between these layers represent the influence of CFC. This approach allows for the analysis of both the modularity of neural activity within specific frequency bands and the interactions between these modules at different frequencies, thereby providing a more comprehensive understanding of the brain's functional organization and dynamic behavior.<sup>18</sup> By considering the brain as a multilayer network, researchers can investigate how information is processed and integrated across multiple spatial and temporal scales, ultimately contributing to a more complete picture of brain function. Understanding these complex within- and cross-frequency interactions is essential for unraveling the mechanisms of neural computation and for gaining insights into the pathophysiology of neurological disorders.19

### A. RQA-based multilayer network representation

The construction of edges within a functional multilayer graph, derived from multichannel M/EEG data, typically involves quantifying synchronization between signals. This synchronization is

a fundamental mechanism for establishing functional connections between neuronal ensembles. Various measures of phase synchronization are commonly employed to assess functional connectivity. However, recent work by Frolov *et al.*<sup>20</sup> has demonstrated the effectiveness of recurrence quantification analysis (RQA) in assessing both within- and cross-frequency synchronization. RQA is a versatile method for analyzing nonlinear time series, which estimates the likelihood of a system revisiting its previous states, i.e., recurrence. Frolov *et al.*<sup>20</sup> demonstrated the potential of RQA measures for detecting CFC, offering an alternative approach to traditional phase-based measures.

However, the cited work<sup>20</sup> focuses primarily on local CFC defined as multiplexed communication between frequency bands within signals from a single sensor (representing a single brain region). Functional connectivity, as a concept, entails the identification of synchronization patterns between distant brain regions that may or may not have direct anatomical connections.<sup>15,21</sup> Therefore, to comprehensively understand inter-regional brain dynamics, it is essential to consider not only CFC within a single region (e.g., between theta and beta bands within the frontal or occipital lobe separately), but also CFC between different regions (e.g., coupling between the theta activity in the frontal cortex and the beta activity in the occipital cortex).

Let us illustrate this approach and the ways of its further modification and development. Figure 1 shows an illustrative example showing the plan of building a network model taking into account cross-frequency connections between different areas. Let us consider signals from three brain regions, frontal (F), parietal (P), and occipital (O) regions, which we will consider in two frequency ranges, theta and beta bands, for certainty, as shown in Fig. 1(a).

Analyzing the connectivity between brain activity signals from different frequency bands and brain regions revealed a set of connections, which is shown in Fig. 1(b). There is an illustration of the resulting multilayer network, where the planes correspond to two frequency bands (theta and beta bands). Accordingly, the lines belonging to the planes characterize the edges within a frequency band. Illustrations of the corresponding adjacency matrices for edges within theta—theta and beta—beta bands, which are symmetric matrices, are shown in Fig. 1(c). The lines that connect nodes on different planes correspond to CFC edges. As can be seen from Fig. 1(c), the CFC analysis results in fundamentally asymmetric adjacency matrices between frequency bands.

To illustrate, consider the example of theta and beta band coupling between frontal and occipital regions. The adjacency matrix would not be symmetric: the strength of coupling between the theta band in the occipital cortex and the beta band in the frontal cortex would be distinct from the coupling between the beta band in the occipital cortex and the theta band in the frontal cortex. This asymmetry highlights the directionality and potentially the causal nature of interactions between different frequency bands across different brain regions.

When constructing a multilayer network from multichannel M/EEG data, a single brain region (or a set of M/EEG sensors) is represented by multiple nodes, each corresponding to a specific frequency band.<sup>22</sup> This raises the question of how to interpret these nodes, which, from a neurophysiological perspective,

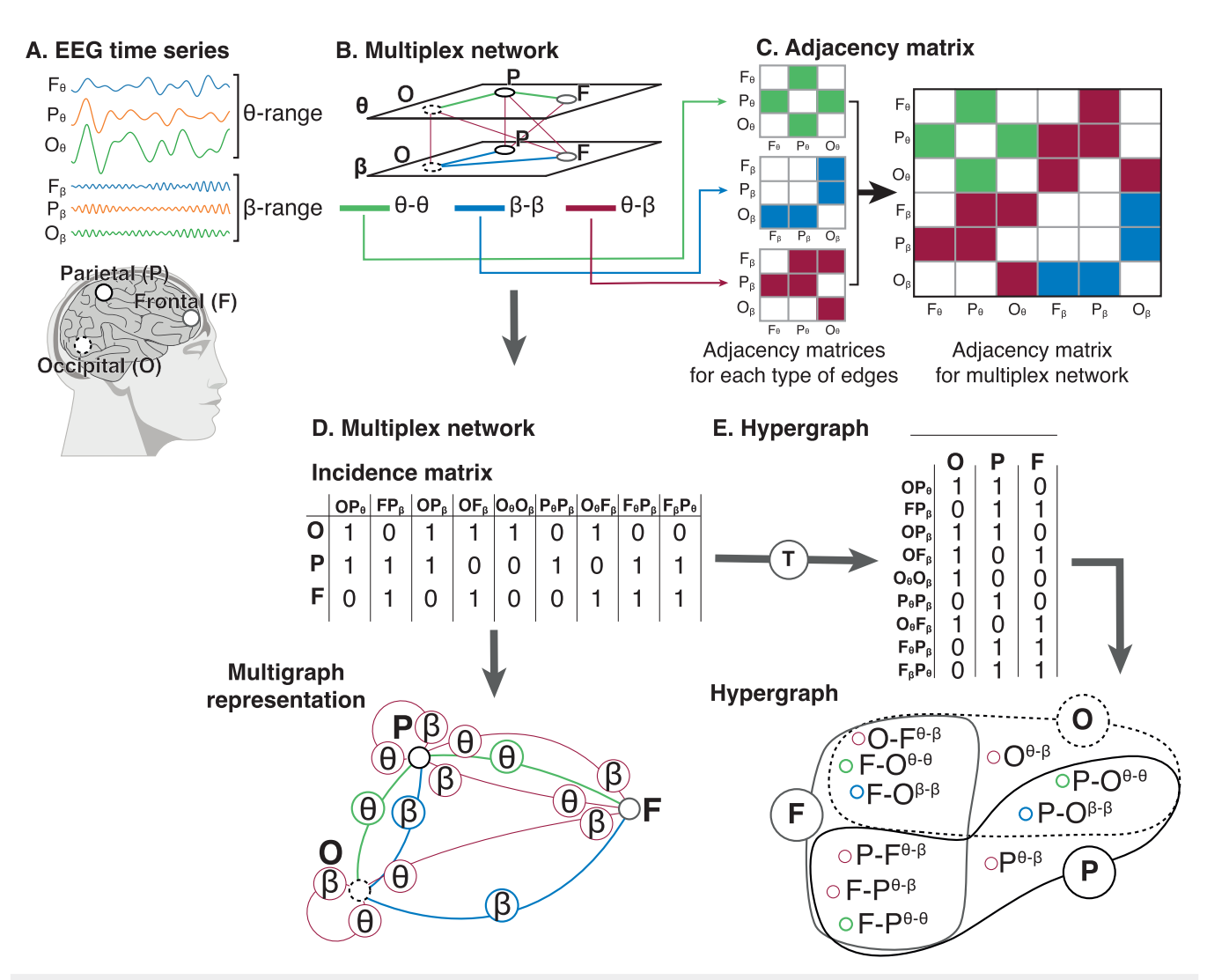


**FIG. 1.** Example of the research pipeline applied to individual EEG sensors. (a) EEG time series (in this example, recorded by F4, P4, and O2 sensors) are filtered in the  $\theta$ -band (top panel) and  $\beta$ -band (middle panel). The bottom panel shows the sensor locations on the human head. (b) A recurrence-based dependency index is computed for each sensor pair in both frequency ranges, forming a two-layer multilayer network. Each layer contains within-frequency connections ( $\theta$ - $\theta$  and  $\beta$ - $\beta$  links), while cross-frequency couplings ( $\theta$ - $\beta$  links) are represented by cross-layer edges. (c) Adjacency matrix of the multiplex network, with cell colors corresponding to edge colors in the network. (d) Multigraph representation of the multilayer network, where within- and cross-layer connections are depicted as distinct edge types, alongside the corresponding incidence with representations are color-coded, e.g.,  $\theta$ - $\theta$  connections are shown in green in the multiplex network, in the adjacency matrix, in the multigraph representation, and as the corresponding node in the hypergraph.

represent the same brain region but are functionally distinct in the network depending on their involvement in within- and cross-frequency interactions [see Figs. 1(b) and 1(c)]. In this framework, each node associated with a brain region, along with its connections, captures the diverse functional roles of that region within the broader network, reflecting its participation in both within- and cross-frequency dynamics.

To avoid duplicating nodes, it would be advantageous to develop a mathematical formalism that maps each brain region to

a single object in the functional brain network, while allowing for multiple types of connections between nodes. This can be achieved using a multigraph **G**, where pairs of nodes can be connected by multiple edges [see Fig. 1(d)]. However, this approach introduces the challenge of analyzing multiple connections between node pairs, requiring the development of methods to evaluate and diagnose multigraph measures. Such measures could be critical for classifying brain states or distinguishing patient groups based on the properties of their functional brain networks.

#### B. Hypergraph representation of a multilayer network

In the analysis of multiplex networks, the traditional approach involves embedding edges into distinct layers based on their type. <sup>16,23</sup> However, hypergraphs offer a more efficient representation of complex higher-order interactions compared to traditional pairwise networks, <sup>24–26</sup> particularly for group interactions. A widely used method is hypergraph projection, which maps a graph to a hypergraph by preserving the node set and converting cliques into hyperedges. <sup>27,28</sup> The primary objective of this process is to maintain the structural integrity of the original graph. Nevertheless, this approach has limitations, including the potential loss of information about the original connectivity when using clique-based mappings. <sup>28</sup>

Our approach is as follows. We treat the edges of the multigraph G [see Fig. 1(d)] as vertices of a new graph, where the number of vertices equals the number of edges in G. These new vertices (representing the edges of G) are connected through the original vertices of G. Mathematically, this is equivalent to transposing the incidence matrix of G. For example, all edges of the multigraph G originating from vertex "1" are connected through this vertex, and in the new graph, the corresponding vertices (representing these edges) are linked by an edge associated with vertex "1." This construction inherently forms a hyperedge spanning multiple vertices, resulting in a hypergraph H. Here, the number of vertices in H equals the number of edges in the multilayer network, and the number of hyperedges corresponds to the number of brain regions used to reconstruct the functional brain network.

A toy illustration of our approach is shown in Figs. 1(d) and 1(e). Since the adjacency matrix of the multiplex network [Fig. 1(c)] does not adequately capture its multiplex structure, we instead use the incidence matrix  $A_G$  of the multigraph G [Fig. 1(d)]. This matrix represents three nodes (O, P, and F) connected by nine edges of different types. To move beyond the multigraph structure while preserving higher-order interactions, we construct a dual hypergraph H to the original multiplex graph G, treating G as a two-uniform hypergraph (where hyperedges connect exactly two vertices). This is achieved by transposing the incidence matrix  $A_G$ , converting edges of G into vertices of H and vertices of G into hyperedges of H [Fig. 1(e)]. Hence, each hyperedge  $e_H$  linking a set of vertices  $V(e_H) \in V$  means that in the original graph **G**, a vertex  $v_{e_H}$ had a corresponding set of incident edges  $E_{V(e_H)}$ . As the hypergraph H is derived from a pairwise interaction network, its vertices have a maximal degree of 2. The described procedure is fully reversible: the original multiplex structure can be recovered by transposing the hypergraph incidence matrix  $A_H$  back to its initial form.

This hypergraph construction resolves the issue of multiple representations of the same region in the adjacency matrix [Fig. 1(c)] and eliminates duplicate edges between nodes in the multigraph [Fig. 1(d)]. By applying topological measures to the hypergraph, we can derive a feature vector for classifying brain states.

### C. Application to autism spectrum disorders

The application of advanced analytical methodologies to study functional brain networks in children with ASD lies at the intersection of complex network theory, computational neuroscience, and clinical medicine. In this study, we apply the introduce approach to analyze higher-order interactions in functional brain networks derived from resting-state EEG data collected from typically developing children and children diagnosed with autism. This research addresses the urgent need for early and objective diagnostic tools for ASD, a neurodevelopmental condition characterized by social communication deficits, restricted interests, and repetitive behaviors.<sup>29</sup>

From a biomedical perspective, this task is critically important. Disrupted functional connectivity—defined as the temporal correlation between spatially remote brain regions—has been consistently identified as a hallmark of ASD.<sup>30–33</sup> These disruptions are thought to underlie the heterogeneous clinical manifestations of ASD, making the development of robust methods for analyzing and diagnosing functional brain networks in children with ASD both a mathematical challenge and a medical necessity. Early diagnosis and intervention are essential for improving long-term outcomes, and the identification of reliable biomarkers through advanced network analysis could significantly enhance diagnostic accuracy and therapeutic targeting.

This study has three primary objectives. First, we apply a RQA-based approach to construct edges of a multilayer graph from multichannel EEG data, capturing both within-frequency and crossfrequency connectivity to comprehensively represent the brain's functional architecture. Second, we investigate the potential of a hypergraph construction procedure based on a multilayer network model to uncover hidden patterns and features in complex networks that traditional graph-theoretical methods may miss. By leveraging higher-order interactions in hypergraphs, we aim to reveal novel insights into the organizational principles of functional brain networks in ASD. Third, we aim to distinguish autism-specific functional hypergraph patterns from those associated with neurotypical development using hypergraph classification techniques applied to resting-state EEG data. Identifying unique topological features of functional hypergraphs in children with ASD could contribute to a diagnostic framework capable of differentiating ASD from typical development with high sensitivity and specificity.

#### II. METHODS

The pipeline of the research is presented in Fig. 2. In this section, we describe the main steps and methods in detail.

## A. Dataset

The dataset comprised resting-state EEG signals from 533 subjects divided into two groups: 282 typically developing children (TD group, 7.2  $\pm$  3 years) and 251 children with autism spectrum disorder (ASD group, 6.7  $\pm$  3.2 years). Detailed inclusion/exclusion criteria (including ADOS-2, CARS, and non-verbal Wechsler scores) are available in the supplementary material.

EEG recordings were acquired using a 19-electrode setup arranged according to the 10–20 international system,<sup>34</sup> with electrodes on the left and right mastoids serving as the reference for a unipolar montage. Subjects were seated comfortably, instructed to remain still with their eyes open, and monitored by their parents to ensure cooperation. Each recording lasted approximately 5 min, sampled at 250 Hz.

Prior to analysis, the data underwent artifact removal using independent component analysis and a 1-125 Hz band-pass filter.

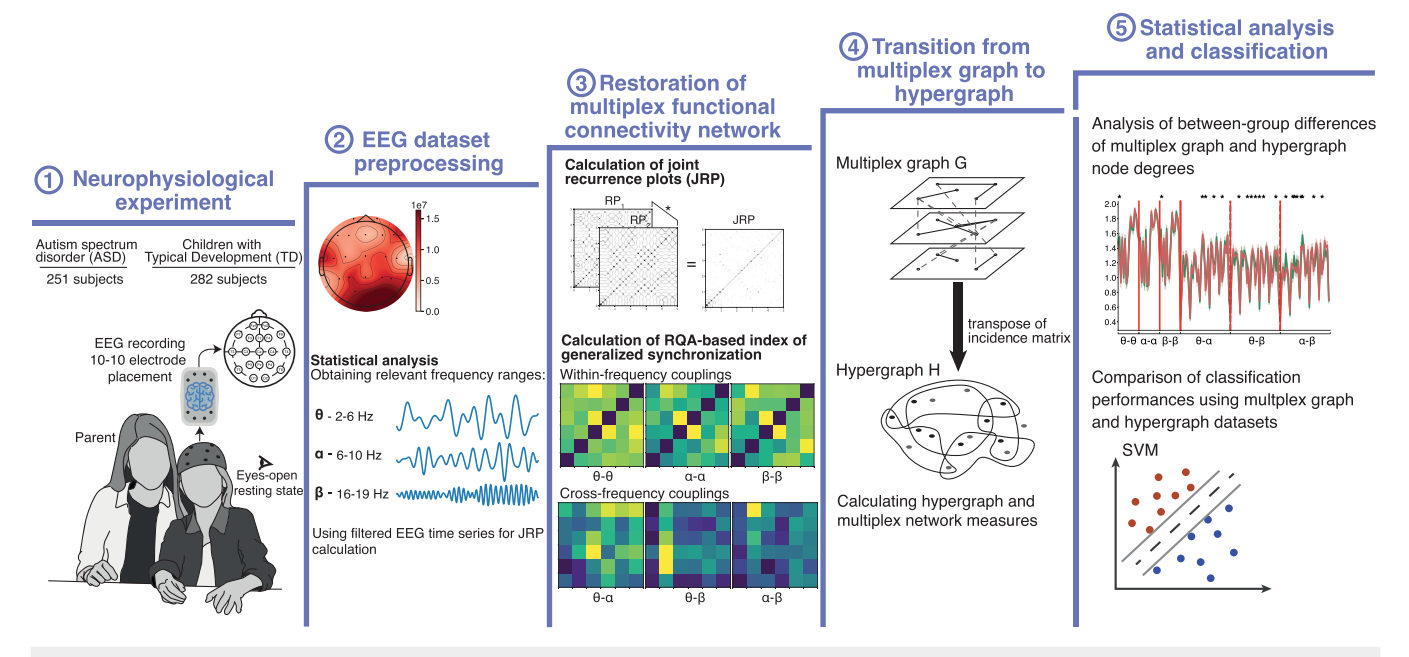


FIG. 2. Research pipeline overview: (1) Experimental dataset of eyes-open resting-state EEG signals from two subject groups, (2) preprocessing and frequency analysis using continuous wavelet transform with statistical testing, (3) reconstruction of multilayer functional connectivity networks via RQA-based methodology, (4) transformation from a three-layer multiplex network to hypergraph representation, and (5) a between-group statistical comparison of multiplex and hypergraph network features and SVM classification using feature vectors from both representations.

Due to challenges in obtaining EEG recordings from autistic children, recording durations varied, with the shortest being 10 s. As recurrence quantification analysis is well-suited for short time series, a random 2-s segment was extracted from each subject's recording for further analysis.

## **B.** Ethical statement

This study was conducted in accordance with the principles of the Declaration of Helsinki. The research methodology was approved by the ethics committee of the Institute of Higher Nervous Activity and Neurophysiology of the Russian Academy of Sciences (protocol No. 2 of April 30, 2020). The parents of all children signed informed consent to participate in this study. Children gave verbal consent to participate.

#### C. Time-frequency analysis

To analyze between-subject differences in brain activity, we computed power spectra for each EEG time series (1–40 Hz) using continuous wavelet transform with a Morlet mother wavelet. This identified frequency ranges of interest (FOIs) showing significant differences between ASD and TD groups. A spatial-frequency permutation cluster-based F-test<sup>36</sup> revealed two significant clusters: slow-frequency (1–10 Hz, p = 0.001) and mid- $\beta$  (16–19 Hz, p = 0.006), both exhibiting increased spectral power in ASD children (see Fig. S1 in the supplementary material).

We determined group-averaged peak alpha frequency (PAF) as the maximum magnitude within the alpha band,<sup>37</sup> finding 8 Hz for TD and 7 Hz for ASD groups. This aligns with established developmental trends where PAF increases from  $\sim\!6\,\text{Hz}$  in infancy to  $\sim\!10\,\text{Hz}$  in adolescence,  $^{38,39}$  and with reported PAF reductions in ASD children.  $^{40,41}$ 

Based on these results, we defined three FOIs:

- $\theta$  range (2–6 Hz);
- slow  $\alpha$  range (6–10 Hz), adjusted for age and PAF differences; and
- mid- $\beta$  range (16–19 Hz).

This selection captures both the identified spectral differences and known developmental characteristics of the groups.

#### D. Recurrence-based multilayer connectivity

In this study, we estimated sensor-level functional connectivity using a measure based on joint recurrence plots (JRPs) introduced in Ref. 42. Building on our previous methodology applied to EEG data, <sup>20</sup> we constructed frequency-specific multilayer functional networks based on the previously identified FOIs. The complete implementation pipeline of this approach is shown in Fig. 3.

## 1. Multivariate embedding

Recurrence plots (RPs) are used to analyze recurrences in *m*-dimensional phase space trajectories of dynamical systems using a two-dimensional visual representation in a form of squared binary matrix *R*.

$$\mathbf{R}_{i,j}^{x} = \Theta(\varepsilon_i - ||\mathbf{x}_i - \mathbf{x}_j||), x_i \in \mathbb{R}, i, j = 1, \dots, N,$$
 (1)

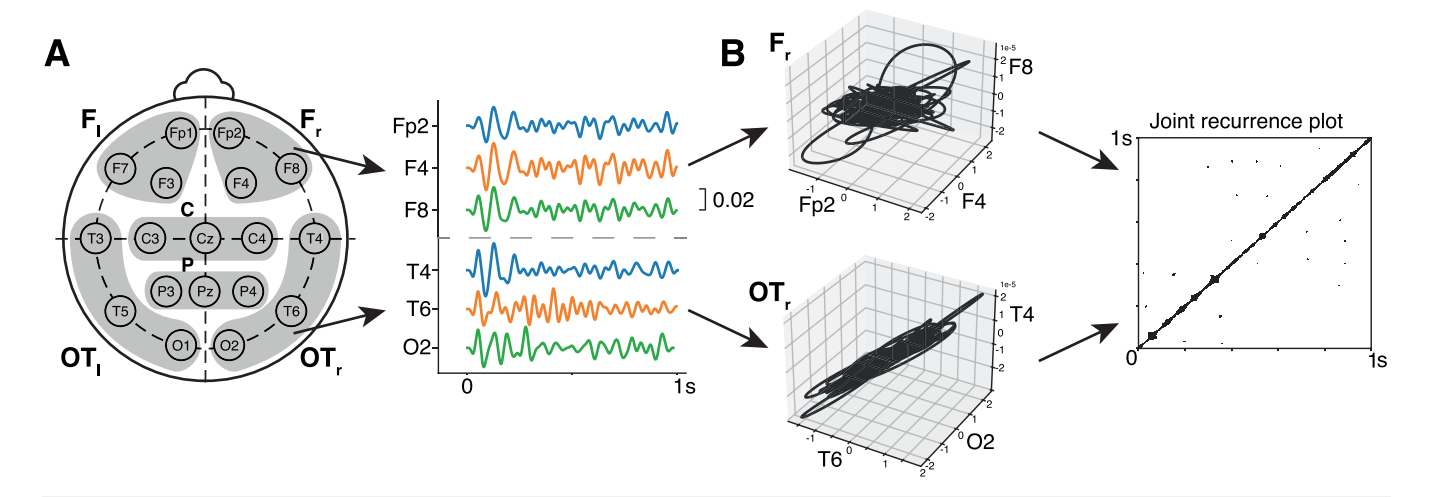


**FIG. 3.** RQA-based functional connectivity estimation: (a) Sensor layout with highlighted triads (gray) used within the multivariate approach, showing exemplary time series from right frontal ( $F_r$ ) and occipito-temporal ( $OT_r$ ) regions. (b) Corresponding 3D state space trajectories and their joint recurrence plot.

where N is the number of states  $\mathbf{x}_i$  (or length of considered time series),  $\varepsilon$  is a threshold that determines the size of the neighborhood centered at  $\mathbf{x}_i$ ,  $||\cdot||$  is the norm, and  $\Theta$  is the Heaviside function.

RPs can be estimated from the time series. The convenient approach of RP calculation is to reconstruct the features of the phase space using an embedding dimension and delay. 43–45 In the present research, however, we employ a multivariate approach rather than Takens' embedding for several reasons. First, using EEG time series to reconstruct a phase space trajectory is problematic since the recorded EEG signal may not robustly represent an underlying dynamical system, which means that the reconstructed phase space portrait is critically dependent on the observed process. 46 Second, when working with sensor-level EEG-based connectivity, one must consider the field spread problem, 15,47 which significantly alters the results of functional connectivity network restoration. Therefore, we group 19 EEG sensors (excluding the Fz sensor) into 3D subsets based on six regions of interest [ROIs, see Fig. 3(a)]:

- 1. Frontal left (*F*<sub>1</sub>): Fp1, F7, F3;
- 2. Frontal right  $(F_r)$ : Fp2, F8, F4;
- 3. Central (C): C3, Cz, C4;
- 4. Parietal (P): P3, Pz, P4;
- 5. Occipito-temporal left  $(OT_l)$ : T3, T5, O1; and
- 6. Occipito-temporal right  $(OT_r)$ : T4, T6, O2.

Therefore, each brain ROI is represented by a 3D state space trajectory [see Fig. 3(b)]. The same multivariate approach was previously used in Ref. 48 and was shown to effectively represent RQA-based effects on EEG signals related to motor execution.

### 2. JRP-based synchronization measure

Joint recurrence plots (JRPs) quantify similarities between two processes  $\mathbf{x}(t)$  and  $\mathbf{y}(t)$  through their recurrence structures.<sup>49</sup> The JRP matrix is computed via element-wise multiplication of individual recurrence matrices from Eq. (1). For each process, the different

thresholds  $\varepsilon$  should be considered, but in the case with JRP calculation, using a fixed number of nearest neighbors  $N_N$  is more appropriate. We fix  $N_N/N$  at the same value for both considered processes ( $RR = N_N/N$ ) and calculate joint recurrence rate as follows:

$$JRR = \frac{1}{N^2} \sum_{i=1}^{N} \sum_{j=1}^{N} \mathbf{J} \mathbf{R}_{i,j},$$
 (2)

where

$$\mathbf{J}\mathbf{R} = \mathbf{R}_{i,i}^{x} \mathbf{R}_{i,i}^{y} \tag{3}$$

is a corresponding joint recurrence matrix. Hence, we can calculate the recurrence-based index of synchronization,

$$S^{xy} = \frac{JRR}{RR}. (4)$$

The value of  $S^{xy}$  indicates the level of similarity between two recurrence matrices and, therefore, the presence of a functional relationship between two processes  $\mathbf{x}(t)$  and  $\mathbf{y}(t)$ .  $S^{xy}$  takes values between 0 (independent processes) and 1 (generalized synchronization, GS).

## E. Cross-frequency coupling and a multilayer network

We construct a multilayer network with nodes representing the six ROIs [Fig. 3(a)] characterized by 3D EEG signals in three defined FOIs. The recurrence-based synchronization index (4) yields:

- Three symmetric within-frequency adjacency matrices (6 × 6):  $\mathbf{W}^{\theta-\theta}$ ,  $\mathbf{W}^{\alpha-\alpha}$ , and  $\mathbf{W}^{\beta-\beta}$  with zeros on main diagonals (no self-loops).
- Three non-symmetric cross-frequency matrices:  $\mathbf{W}^{\theta-\alpha}$ ,  $\mathbf{W}^{\theta-\beta}$ , and  $\mathbf{W}^{\alpha-\beta}$ .

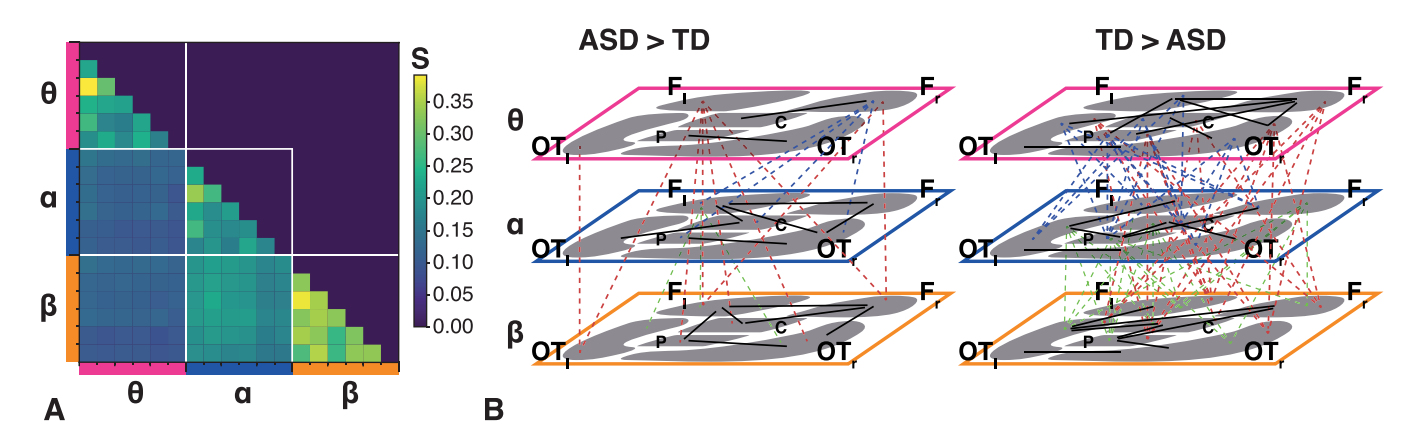


**FIG. 4.** Multilayer network analysis: (a) Adjacency matrix of the three-layer multiplex network, with within-frequency connections (diagonal blocks) and cross-frequency couplings (lower triangle). (b) Results of between-group network-based statistics showing significantly stronger connections in the ASD (left) and TD (right) groups  $(t_{critical} = 3.05, p_{critical} = 0.001)$ .

The super-adjacency matrix for a multilayer graph G of size  $(18 \times 18)$  is defined as the block matrix,

$$\mathbf{S}_{\mathbf{G}} = \begin{pmatrix} \mathbf{W}^{\theta-\theta} & 0 & 0 \\ \mathbf{W}^{\theta-\alpha} & \mathbf{W}^{\alpha-\alpha} & 0 \\ \mathbf{W}^{\theta-\beta} & \mathbf{W}^{\alpha-\beta} & \mathbf{W}^{\beta-\beta} \end{pmatrix},\tag{5}$$

where diagonal blocks encode intra-layer within-frequency connectivity and off-diagonal blocks represent CFCs [Fig. 4(a), lower half shown due to symmetry].

Network-based statistics<sup>50</sup> (NBS;  $t_{critical} = 3.05$ ,  $p_{critical} = 0.001$ ) reveal distinct connectivity patterns [Fig. 4(b)]:

- TD group: Stronger overall connectivity compared to the ASD group.
- *ASD group*: Dominant within-frequency connections (right frontal/occipito-temporal to central/parietal) and stronger CFC between the bilateral frontal cortex in the  $\theta$ -layer and almost all other areas in  $\alpha$  and  $\beta$ —layers compared to the TD group.

These findings align with the conflicting literature on ASD connectivity, where both hyper- and hypo-connectivities have been reported, 51,52 suggesting limitations of functional connectivity as a standalone biomarker. 53

## F. Classification

To demonstrate the advantages of a hypergraph representation over conventional multiplex networks, we implemented a support vector machine (SVM) classifier using node degree features extracted from both representations.

The classification pipeline incorporated rigorous validation measures to prevent overfitting:

- Hyperparameter tuning through grid search, which has been empirically validated for improving classification performance while controlling overfitting.<sup>54-56</sup>
- 2. Model evaluation using a tenfold cross-validation technique.<sup>57</sup>

The optimal hyperparameters identified through the grid search were:

- Regularization parameter C = 1 for a multiplex network and C = 10 for a hypergraph.
- Kernel coefficient  $\gamma=0.005$  for a multiplex network and  $\gamma=0.01$  for a hypergraph.
- · RBF kernel for both models.

Among all hyperparameters, the regularization parameter C and kernel parameter  $\gamma$  have the greatest impact on SVM performance. In particular,  $\gamma$  affects the sample data mapping, and C controls the "compromise" between the maximization of the margin and minimization of the training error. S

Feature vectors consisted of:

- 18-dimensional degree vectors for multiplex networks (6 nodes × 3 layers).
- 153-dimensional degree vectors for hypergraphs (comprising 15 within-frequency hypergraph nodes per layer and 36 cross-frequency nodes between each layer pair).

## III. RESULTS AND DISCUSSION

## A. Hypergraph construction

To analyze the RQA-based adjacency matrices, we applied a series of thresholds to systematically prune the weakest connections, retaining only edges above specified quantiles q = [0.4, 0.5, 0.6, 0.7, 0.8, 0.9, 0.95, 0.975] of the initial edge weight distribution. Each weighted connection  $S_{ij}$  in the super-adjacency matrix [Eq. (5)] was binarized according to

$$a_{ij} = \begin{cases} 0, & S_{ij} < q, \\ 1, & S_{ij} > q. \end{cases}$$
 (6)

Following this thresholding procedure, we derived for each participant the incidence matrix  $A_G$  of the thresholded multilayer network and its corresponding hypergraph incidence matrix  $A_H$ 

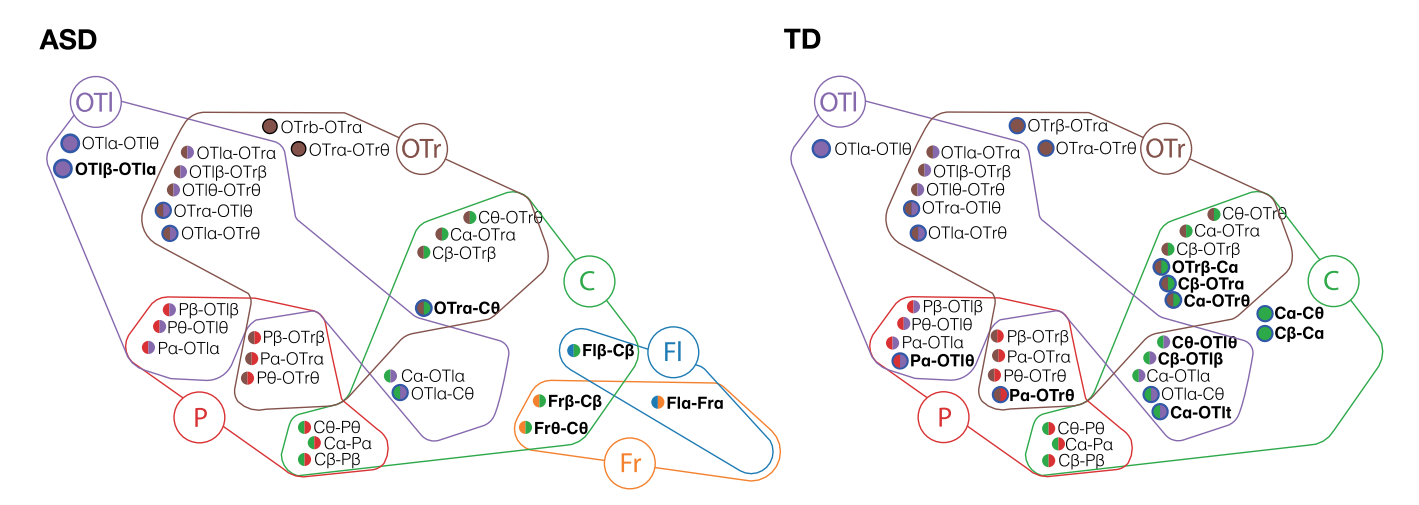


**FIG. 5.** Consensus hypergraphs for ASD and TD groups at threshold q=0.5, where closed colored contours represent hyperedges. Nodes present in only one group are highlighted in bold. Each node's name corresponds to its original connection in the multilayer network prior to hypergraph conversion—for example, node  $OTI_{\alpha} - OTI_{\beta}$  represents the edge connecting the OTI region between  $\alpha$ - and  $\beta$ -layers in the initial multilayer network. Node colors indicate their membership in specific hyperedges.

obtained through matrix transposition,

$$\mathbf{A}_H = \mathbf{A}_G^T. \tag{7}$$

Each resulting hypergraph contained E=6 hyperedges corresponding precisely to the ROIs defined in Sec. II D 1.

To visualize group-level patterns, we generated consensus hypergraphs for both ASD and TD groups, <sup>59</sup> retaining only nodes that are present in at least 50% of subjects in each group. The procedure involves averaging the binarized connections in the incident matrix  $\mathbf{A}_H$  over all subjects in the group,

$$a_{ij}^* = \frac{1}{N} \sum_{n=1}^{N} a_{ij}^n, \tag{8}$$

where n is the subject number and N is the number of subjects in the group. Finally, to construct consensus incidence matrix  $\tilde{A}_H$ , we binarize the resulting connection strengths as follows:

$$\tilde{a}_{ij} = \begin{cases} 0, & a_{ij}^* < 0.5, \\ 1, & a_{ij}^* > 0.5. \end{cases}$$
 (9)

This consensus approach, which has demonstrated particular utility in studying the topology of fMRI-based functional brain networks,  $^{59\text{-}61}$  revealed striking between-group differences (Fig. 5). The ASD group exhibited robust preservation of within-frequency connectivity in bilateral frontal regions across all frequency bands  $(\beta-\beta,~\alpha-\alpha,~\text{and}~\theta-\theta)$  and relatively sparse cross-frequency coupling outside frontal areas. In contrast, the TD group showed more distributed patterns of cross-frequency coupling, prominent CFC involving central and occipito-temporal regions, and greater overall integration across frequency bands. These findings highlight how the hypergraph representation captures organizational principles that may be obscured in conventional multilayer

network analyses, particularly the distinct balance between withinfrequency and cross-frequency interactions in neurotypical vs ASD populations.

## B. Statistical analysis of a multilayer network and hypergraph measures

We chose node degrees to compare the ability of both multiplex and hypergraph representations to identify differences between functional connectivity of ASD and TD groups of subjects. Without applying threshold, each multilayer network of brain functional connectivity was fully connected with total 153 edges (15 edges in each within-frequency layer and 36 × 3 cross-frequency couplings between layers), with a value of S indicating the strength of synchronization between nodes. The thresholding procedure removed the less important edges and opened the possibility to highlight the differences between ASD and TD groups by analyzing the features of corresponding network structures. Before proceeding with the t-test, the normality assumptions were verified for both datasets (hypergraph and multiplex networks). Additionally, the corresponding p-values were adjusted to account for multiple hypothesis testing using the Benjamini-Hochberg test.<sup>62</sup> Figure 6 shows the result of the t-test for independent samples for both hypergraph and multiplex network node degrees for q = 0.9. P-values for each quantile are presented in Tables S1 and S2 of the supplementary material.

Our analysis revealed that the hypergraph representation provided superior discriminative capability compared to the conventional multiplex network approach. Specifically, while connection-type-averaged degrees failed to show any significant between-group differences in the multiplex networks regardless of threshold selection, the hypergraph representation successfully identified statistically significant divergence in nodes that predominantly involved  $\theta$ - $\alpha$  connectivity patterns. This finding underscores the enhanced

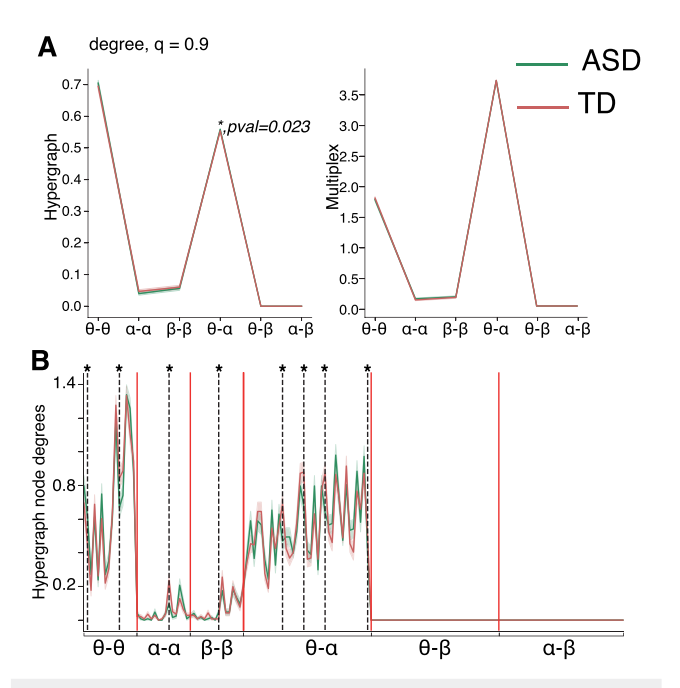


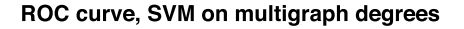
**FIG. 6.** Statistical comparison of network measures at threshold q=0.9. (a) Group-averaged node degrees stratified by connection type (within-frequency and cross-frequency couplings for all bands), shown for both hypergraph (left) and multiplex network (right) representations. (b) Local node degree distributions (mean  $\pm$  SD) in the hypergraph representation, where asterisks (\*) mark nodes showing statistically significant between-group differences.

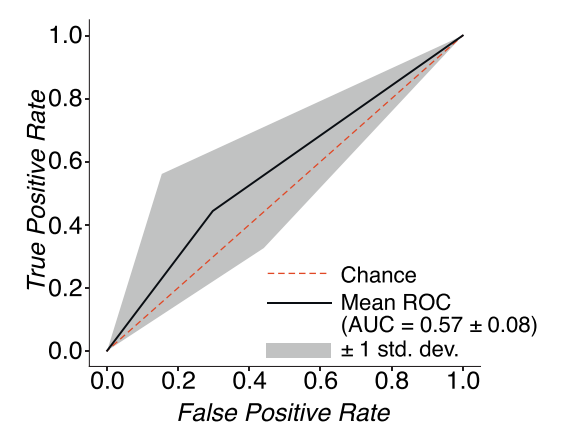
sensitivity of hypergraph-based measures for detecting neurophysiologically relevant differences in functional network organization between ASD and TD populations.

#### C. Classification

The statistically significant between-group differences revealed by our analysis suggest promising avenues for improving ASD classification performance. Current clinical practice relies heavily on behavioral observations and parental questionnaires, which while effective for diagnosis by age  $2^{63}$  could benefit from complementary quantitative biomarkers. The importance of such objective measures is underscored by research showing that early intervention outcomes correlate positively with treatment efficacy,  $^{64}$  highlighting the need for reliable auxiliary diagnostic tools.  $^{65}$ 

The classification performance, as shown in Fig. 7, reveals a clear superiority of hypergraph-derived features. While the achieved metrics (F1-score: 81%, AUC: 0.81) may not represent the absolute state-of-the-art in ASD classification, they demonstrate clinically meaningful potential. These results suggest that the method could serve as a valuable supplementary tool for diagnostic confirmation, treatment monitoring, and research into ASD connectivity patterns. The ROC curves in Fig. 7 provide visual confirmation of the hypergraph's discriminative power, with multiplex network features showing minimal ability to distinguish between diagnostic groups. This pronounced performance difference underscores





#### ROC curve, SVM on hypergraph degrees

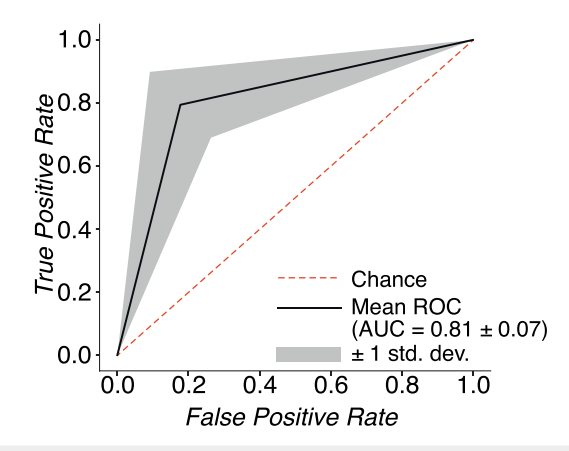


**FIG. 7.** Receiver operating characteristic (ROC) analysis of SVM classifiers trained on different network representations. The left panel shows performance using multiplex network features, while the right panel displays results for hypergraph-derived features. Plots show the mean ROC curve with standard deviatrea across all k-fold cross-validation iterations, with the corresponding area under the curve (AUC) scores indicating overall classification performance. The shaded regions represent the  $\pm 1$  standard deviation of the ROC curves across validation folds.

the critical importance of a network representation choice when analyzing functional connectivity in neurodevelopmental disorders.

There is a vast amount of research dedicated to ML-based identification of ASD children based on the brain functional connectivity measures, many of which present an impressive performance of classifiers. Considering the pairwise interactions, in Ref. 66, the authors demonstrated 95.8% accuracy, 100% sensitivity, and 92% specificity via SVM. The authors of this paper calculated the brain connectivity network in the several frequency bands and, unlike this article, considered them separately from each other. The authors of Ref. 67 employed discrete wavelet transform and correlation-based feature selection to achieve accuracy of 93% via random forest. Another SVM study<sup>68</sup> achieved 85.4% accuracy via SVM trained on relative

power indices calculated using FFT on EEG data. Impressive 99.15% accuracy was achieved by applying short-term Fourier Transform to get 4657 spectral images based on EEG and a trained CNN-based classifier.  $^{69}$ 

While pairwise interaction studies are mostly focused on the efficiency of classification, the research on higher-order interactions is more interpretation-oriented and has an emphasis on the ability of hypergraph construction methods to reveal novel differences in higher-order network structures between normal and pathological brain networks. However, there is a rather limited amount of ASD research dedicated to higher-order interactions, including MLbased classification. In Ref. 70, the authors proposed a method based on hypergraph convolution and gated attention with a maximum AUC of 77.03. Another contrastive learning method described in Ref. 71 reached AUC = 64.8. In Ref. 72, the authors proposed an approach for hypergraph construction from fMRI time series that achieves a classification accuracy of 80.31%. Outside of ASD detection and identification, hypergraph-based approaches are being actively applied to reveal various cognitive processes in the brain that may be omitted in the pairwise approach.<sup>73</sup>

In the present study, an AUC of 81 was achieved using an SVM-based classifier trained on hypergraph measures. Our results demonstrate that converting multiplex networks to hypergraph representations yields substantial advantages for machine learning applications. The hypergraph transformation not only increases feature dimensionality from 18 to 153 features but, more importantly, captures statistically significant between-group differences that are absent in the multiplex representation. We evaluated these advantages by training SVM classifiers using local node degree features from both network types.

# D. Enhanced stability of connectivity patterns in a hypergraph representation

The hypergraph approach demonstrates fundamentally greater stability in capturing group-level connectivity patterns compared to traditional multilayer network representations This critical advantage emerges from intrinsic differences in how topological information is structured across the two frameworks. To illustrate this phenomenon, consider a characteristic ASD connectivity pattern, shown for simplicity as a triangle ABC within a multilayer network, where A, B, and C represent specific nodes. In conventional multiplex network analysis, each node of this pattern would exhibit a nominal degree of 2, yet display substantial intersubject variability with potential degree values spanning from 0 to 17 (due to the presence of 3 frequency layers and 6 regional nodes per layer). This pronounced variability stems from two primary sources: the stochastic inclusion of extraneous connections beyond the core pattern and the intermittent absence of essential pattern-defining connections in individual subjects.

The transformation to hypergraph representation induces a paradigm shift in pattern stability. Each connection within the original pattern transitions into an autonomous node with deterministic degree properties—specifically degree 2 for connections between different brain regions and degree 1 for cross-frequency couplings between representations of the same region in different frequency layers. This transformation yields three fundamental

stabilizing characteristics. First, the core connectivity pattern maintains structural invariance regardless of additional random connections that may appear in individual subjects. Second, the representation demonstrates inherent noise resistance, as extraneous connections external to the pattern leave the degrees of pattern nodes unaffected. Third, and most consequentially, the metric dispersion shows marked reduction across subjects for hypergraph-derived measures compared to multiplex network metrics.

These theoretical advantages manifest concretely in our empirical results, accounting for both the enhanced statistical significance and superior classification accuracy observed with hypergraph-derived features. The framework's capacity to isolate essential connectivity patterns from incidental variations explains its robust performance. Where multiplex networks conflate meaningful connectivity with random variations, hypergraphs effectively decouple these components, preserving a clean pattern representation despite biological variability. This property proves particularly valuable in clinical applications where distinguishing consistent neurophysiological signatures from individual variations is paramount. Our quantitative comparisons reveal substantially tighter clustering of hypergraph features across subjects, directly translating to more reliable group discrimination and clinical classification potential.

#### IV. CONCLUSION

In this study, we propose an approach for distinguishing ASD using advanced methods of functional connectivity analysis applied to neurophysiological EEG data. Our research prioritized detectability over interpretability, aiming to uncover functional connectivity features that could enhance the robustness of diagnostic classifiers. The key innovation of our work lies in the transition from a frequency-based functional connectivity multilayer network to a hypergraph representation. This transformation is lossless, reversible, and significantly improves classification performance, offering a new perspective on the analysis of complex brain networks.

First, we demonstrated that representing brain networks as hypergraphs, rather than traditional multilayer networks, allows for the detection of higher-order interactions that are not captured by conventional graph-theoretical methods. This approach revealed unique topological features in the functional brain networks of children with ASD, which were not apparent in the multilayer network representation. Second, the hypergraph-based features provided statistically significant differences between ASD and TD groups, leading to a considerable improvement in classification performance. Using an SVM classifier, we achieved an F1-score of 81% with hypergraph features, compared to only 57% with multilayer network features. This suggests that hypergraph measures are more stable and informative for distinguishing ASD from TD. Third, our analysis revealed distinct patterns of functional connectivity in children with ASD, particularly in bilateral frontal regions within specific frequency bands. These findings align with previous studies that have reported both increased and decreased connectivity in ASD, highlighting the complexity of neural connectivity in this disorder.

Future work will focus on improving the interpretability of hypergraph measures by exploring their topological properties in greater detail, potentially through the development of new metrics

or visualization techniques that bridge the gap between complex network theory and clinical neuroscience. We also plan to expand our analysis to larger and more diverse datasets, including longitudinal studies, to validate the robustness of our approach across different populations and developmental stages. This expansion will enable us to explore potential subtypes of ASD and their unique connectivity profiles, providing a more nuanced understanding of the disorder. Additionally, integrating EEG data with other neuroimaging modalities, such as fMRI or structural MRI, could offer a more comprehensive understanding of the neural mechanisms underlying ASD. This multimodal approach may enhance the accuracy and interpretability of diagnostic classifiers, further refining our ability to detect and monitor ASD.

In conclusion, our study represents a step forward in the application of advanced network analysis techniques to the study of ASD. By leveraging hypergraph representations, we have uncovered new insights into the functional connectivity patterns associated with ASD. While challenges remain, particularly in terms of interpretability and generalizability, our findings highlight the potential of hypergraph-based approaches to transform the field of neurodevelopmental disorder research.

#### SUPPLEMENTARY MATERIAL

See the supplementary material that provides additional details supporting the main research paper. It includes:

- Inclusion/exclusion criteria: Clear guidelines for participant selection, ensuring rigorous group comparisons (ASD vs typically developing children).
- Figure S1: Statistical results from EEG frequency analysis, highlighting significant differences in brain activity (1-10 Hz and 16-19 Hz ranges) between groups.
- Tables S1 and S2: Statistical comparisons of brain network connectivity (node degrees) across different thresholds, contrasting multiplex network and hypergraph representations.

## **ACKNOWLEDGMENTS**

This work was supported by the Russian Science Foundation (Grant No. 23-71-30010).

## **AUTHOR DECLARATIONS**

## **Conflict of Interest**

The authors have no conflicts to disclose.

### **Author Contributions**

Elena Pitsik: Formal analysis (equal); Investigation (equal); Methodology (equal); Software (equal); Validation (equal); Visualization (equal); Writing - original draft (equal); Writing - review & editing (equal). Semen Kurkin: Conceptualization (equal); Investigation (equal); Methodology (equal); Validation (equal); Visualization (equal); Writing - original draft (equal). Olga Martynova: Conceptualization (equal); Data curation (equal); Methodology (equal); Validation (equal); Writing - review & editing

(equal). Galina Portnova: Conceptualization (equal); Data curation (equal); Methodology (equal); Validation (equal); Writing review & editing (equal). Alexander E. Hramov: Conceptualization (equal); Formal analysis (equal); Funding acquisition (equal); Investigation (equal); Methodology (equal); Project administration (equal); Resources (equal); Supervision (equal); Writing - original draft (equal); Writing - review & editing (equal).

#### **DATA AVAILABILITY**

The data that support the findings of this study are available on request from the corresponding author. The data are not publicly available due to privacy and ethical restrictions.

#### REFERENCES

- <sup>1</sup>L. C. Cruikshank, A. Singhal, M. Hueppelsheuser, and J. B. Caplan, "Theta oscillations reflect a putative neural mechanism for human sensorimotor integration," Neurophysiol. 107, 65-77 (2012).
- <sup>2</sup>N. S. Frolov, E. N. Pitsik, V. A. Maksimenko, V. V. Grubov, A. R. Kiselev, Z. Wang, and A. E. Hramov, "Age-related slowing down in the motor initiation in elderly adults," PLoS One 15, e0233942 (2020).
- <sup>3</sup>C. Palmer, L. Zapparoli, and J. M. Kilner, "A new framework to explain sensorimotor beta oscillations," Trends Cognit. Sci. 20, 321–323 (2016).
- <sup>4</sup>V. A. Maksimenko, A. Kuc, N. S. Frolov, M. V. Khramova, A. N. Pisarchik, and A. E. Hramov, "Dissociating cognitive processes during ambiguous information processing in perceptual decision-making," Front. Behav. Neurosci. 14, 95
- <sup>5</sup>R. T. Canolty and R. T. Knight, "The functional role of cross-frequency coupling," Trends Cognit. Sci. 14, 506–515 (2010).

  <sup>6</sup>O. Jensen and L. L. Colgin, "Cross-frequency coupling between neuronal oscilla-
- tions," Trends Cognit. Sci. 11, 267-269 (2007).
- <sup>7</sup>J. E. Lisman and O. Jensen, "The theta-gamma neural code," Neuron 77, 1002-1016 (2013).
- <sup>8</sup>B. Voytek and R. T. Knight, "Dynamic network communication as a unifying neural basis for cognition, development, aging, and disease," Biol. Psychiatry 77, 1089-1097 (2015).
- <sup>9</sup>B. Chen, L. F. Ciria, C. Hu, and P. C. Ivanov, "Ensemble of coupling forms and networks among brain rhythms as function of states and cognition," Commun. Biol. 5, 82 (2022).
- <sup>10</sup>G. Buzsaki, Rhythms of the Brain (Oxford University Press, New York, 2006).
- <sup>11</sup>P. Fries, "A mechanism for cognitive dynamics: Neuronal communication through neuronal coherence," Trends Cognit. Sci. 9, 474–480 (2005).

  12S. Boccaletti, V. Latora, Y. Moreno, M. Chavez, and D.-U. Hwang, "Complex
- networks: Structure and dynamics," Phys. Rep. 424, 175-308 (2006).
- <sup>13</sup>E. Bullmore and O. Sporns, "Complex brain networks: Graph theoretical analysis of structural and functional systems," Nat. Rev. Neurosci. 10, 186-198
- <sup>14</sup>D. Papo, J. M. Buldú, S. Boccaletti, and E. T. Bullmore, "Complex network theory and the brain," Phil. Trans. R. Soc. B 369, 20130520 (2014).
- 15 A. E. Hramov, N. S. Frolov, V. A. Maksimenko, S. A. Kurkin, V. B. Kazantsev, and A. N. Pisarchik, "Functional networks of the brain: From connectivity restoration to dynamic integration," Phys.-Usp. 64, 584 (2021).
- 16S. Boccaletti, G. Bianconi, R. Criado, C. I. Del Genio, J. Gómez-Gardenes, M. Romance, I. Sendina-Nadal, Z. Wang, and M. Zanin, "The structure and dynamics of multilayer networks," Phys. Rep. 544, 1-122 (2014).
- <sup>17</sup>M. Kivelä, A. Arenas, M. Barthelemy, J. P. Gleeson, Y. Moreno, and M. A. Porter, "Multilayer networks," J. Complex Netw. 2, 203-271 (2014).
- 18D. S. Bassett and E. T. Bullmore, "Human brain networks in health and disease," Curr. Opin. Neurol. 22, 340-347 (2009).
- <sup>19</sup>P. J. Uhlhaas and W. Singer, "Neural synchrony in brain disorders: Relevance for cognitive dysfunctions and pathophysiology," Neuron 52, 155-168

- <sup>20</sup>N. Frolov, V. Maksimenko, and A. Hramov, "Revealing a multiplex brain network through the analysis of recurrences," Chaos **30**, 121108 (2020).
- <sup>21</sup>H.-J. Park and K. Friston, "Structural and functional brain networks: From connections to cognition," Science **342**, 1238411 (2013).
- <sup>22</sup>Z. Hammoud and F. Kramer, "Multilayer networks: Aspects, implementations, and application in biomedicine," Big Data Anal. 5, 2 (2020).
- <sup>23</sup>F. Battiston, V. Nicosia, and V. Latora, "Structural measures for multiplex networks," Phys. Rev. F. **89**, 032804 (2014).
- <sup>24</sup>S. Boccaletti, P. De Lellis, C. Del Genio, K. Alfaro-Bittner, R. Criado, S. Jalan, and M. Romance, "The structure and dynamics of networks with higher order interactions," Phys. Rep. 1018, 1–64 (2023).
- <sup>25</sup>G. Burgio, J. T. Matamalas, S. Gómez, and A. Arenas, "Evolution of cooperation in the presence of higher-order interactions: From networks to hypergraphs," Entropy 22, 744 (2020).
- <sup>26</sup>J.-G. Young, G. Petri, and T. P. Peixoto, "Hypergraph reconstruction from network data," Commun. Phys. **4**, 135 (2021).
- <sup>27</sup>Y. Wang and J. Kleinberg, "From graphs to hypergraphs: Hypergraph projection and its remediation," arXiv:2401.08519 (2024).
- <sup>28</sup>M. M. Wolf, A. M. Klinvex, and D. M. Dunlavy, "Advantages to modeling relational data using hypergraphs versus graphs," in 2016 IEEE High Performance Extreme Computing Conference (HPEC) (IEEE, 2016), pp. 1–7.
- <sup>29</sup>C. Lord, T. S. Brugha, T. Charman, J. Cusack, G. Dumas, T. Frazier, E. J. Jones, R. M. Jones, A. Pickles, M. W. State *et al.*, "Autism spectrum disorder," Nat. Rev. Dis. Primers **6**, 5 (2020).
- <sup>30</sup>T.-E. Kam, H.-I. Suk, and S.-W. Lee, "Multiple functional networks modeling for autism spectrum disorder diagnosis," Hum. Brain Mapp. 38, 5804–5821 (2017).
- <sup>31</sup>C. L. Alves, T. G. D. O. Toutain, P. de Carvalho Aguiar, A. M. Pineda, K. Roster, C. Thielemann, J. A. M. Porto, and F. A. Rodrigues, "Diagnosis of autism spectrum disorder based on functional brain networks and machine learning," Sci. Rep. 13, 8072 (2023).
- <sup>32</sup>Y. Xu, Z. Yu, Y. Li, Y. Liu, Y. Li, and Y. Wang, "Autism spectrum disorder diagnosis with EEG signals using time series maps of brain functional connectivity and a combined CNN-LSTM model," Comput. Methods Programs Biomed. 250, 108196 (2024).
- <sup>33</sup> M. S. Kabir, S. Kurkin, G. Portnova, O. Martynova, Z. Wang, and A. Hramov, "Contrastive machine learning reveals in EEG resting-state network salient features specific to autism spectrum disorder," Chaos, Solitons Fractals 185, 115123 (2024).
- <sup>34</sup>A. E. Society, "Guideline thirteen," J. Clin. Neurophysiol. **11**, 111–113 (1994).
- 35 A. E. Hramov, A. A. Koronovskii, V. A. Makarov, A. N. Pavlov, and E. Sitnikova, Wavelets in Neuroscience (Springer, 2015).
- <sup>36</sup>E. Maris and R. Oostenveld, "Nonparametric statistical testing of EEG-and MEG-data," J. Neurosci. Methods **164**, 177–190 (2007).
- <sup>37</sup>S. Haegens, H. Cousijn, G. Wallis, P. J. Harrison, and A. C. Nobre, "Interand intra-individual variability in alpha peak frequency," NeuroImage **92**, 46–55 (2014).
- <sup>38</sup>J. Freschl, L. Al Azizi, L. Balboa, Z. Kaldy, and E. Blaser, "The development of peak alpha frequency from infancy to adolescence and its role in visual temporal processing: A meta-analysis," Dev. Cogn. Neurosci. 57, 101146 (2022).
  <sup>39</sup>M. McSweeney, S. Morales, E. A. Valadez, G. A. Buzzell, L. Yoder, W. P. Fifer,
- <sup>39</sup>M. McSweeney, S. Morales, E. A. Valadez, G. A. Buzzell, L. Yoder, W. P. Fifer, N. Pini, L. C. Shuffrey, A. J. Elliott, J. R. Isler *et al.*, "Age-related trends in aperiodic EEG activity and alpha oscillations during early-to middle-childhood," NeuroImage **269**, 119925 (2023).
- <sup>40</sup> A. Dickinson, C. DiStefano, D. Senturk, and S. S. Jeste, "Peak alpha frequency is a neural marker of cognitive function across the autism spectrum," Eur. J. Neurosci. 47, 643–651 (2018).
- <sup>41</sup> A. Dickinson, K. J. Varcin, M. Sahin, C. A. Nelson, III, and S. S. Jeste, "Early patterns of functional brain development associated with autism spectrum disorder in tuberous sclerosis complex," Autism Res. 12, 1758–1773 (2019).
- <sup>42</sup>M. C. Romano, M. Thiel, J. Kurths, I. Kiss, and J. Hudson, "Detection of synchronization for non-phase-coherent and non-stationary data," Europhys. Lett. 71, 466 (2005).
- <sup>43</sup> M. Matilla-García, I. Morales, J. M. Rodríguez, and M. Ruiz Marín, "Selection of embedding dimension and delay time in phase space reconstruction via symbolic dynamics," Entropy 23, 221 (2021).

- <sup>44</sup>H.-G. Ma and C.-Z. Han, "Selection of embedding dimension and delay time in phase space reconstruction," Front. Electr. Electron. Eng. China 1, 111–114 (2006).
- (2006).

  <sup>45</sup>E. Tan, S. Algar, D. Corrêa, M. Small, T. Stemler, and D. Walker, "Selecting embedding delays: An overview of embedding techniques and a new method using persistent homology," Chaos 33, 032101 (2023).
- <sup>46</sup>C. Letellier, J. Maquet, L. Le Sceller, G. Gouesbet, and L. Aguirre, "On the non-equivalence of observables in phase-space reconstructions from recorded time series," J. Phys. A: Math. Gen. 31, 7913 (1998).
- series," J. Phys. A: Math. Gen. 31, 7913 (1998).

  47 J.-M. Schoffelen and J. Gross, "Source connectivity analysis with MEG and EEG," Hum. Brain Mapp. 30, 1857–1865 (2009).
- <sup>48</sup>E. Pitsik, N. Frolov, K. Hauke Kraemer, V. Grubov, V. Maksimenko, J. Kurths, and A. Hramov, "Motor execution reduces EEG signals complexity: Recurrence quantification analysis study," Chaos **30**, 023111 (2020).
- quantification analysis study," Chaos 30, 023111 (2020).

  49 N. Marwan, M. C. Romano, M. Thiel, and J. Kurths, "Recurrence plots for the analysis of complex systems," Phys. Rep. 438, 237–329 (2007).
- <sup>50</sup> A. Zalesky, A. Fornito, and E. T. Bullmore, "Network-based statistic: Identifying differences in brain networks," NeuroImage 53, 1197–1207 (2010).
- <sup>51</sup>C. O'Reilly, J. D. Lewis, and M. Elsabbagh, "Is functional brain connectivity atypical in autism? A systematic review of EEG and MEG studies," PLoS One 12, e0175870 (2017).
- <sup>52</sup>L. Bogéa Ribeiro and M. da Silva Filho, "Systematic review on EEG analysis to diagnose and treat autism by evaluating functional connectivity and spectral power," Neuropsychiatr. Dis. Treat. **19**, 415–424 (2023).
- power," Neuropsychiatr. Dis. Treat. 19, 415-424 (2023). <sup>53</sup>X. Geng, X. Fan, Y. Zhong, M. F. Casanova, E. M. Sokhadze, X. Li, and J. Kang, "Abnormalities of EEG functional connectivity and effective connectivity in children with autism spectrum disorder," Brain Sci. 13, 130 (2023)
- <sup>54</sup>P. Lameski, E. Zdravevski, R. Mingov, and A. Kulakov, "SVM parameter tuning with grid search and its impact on reduction of model over-fitting," in *Rough Sets, Fuzzy Sets, Data Mining, and Granular Computing: 15th International Conference, RSFDGrC 2015, Proceedings, Tianjin, China, 20–23 November 2015* (Springer, 2015), pp. 464–474.
- 55 H. A. Fayed and A. F. Atiya, "Speed up grid-search for parameter selection of support vector machines," Appl. Soft Comput. 80, 202–210 (2019).
- 56S. Han, C. Qubo, and H. Meng, "Parameter selection in SVM with RBF kernel function," in *World Automation Congress 2012* (IEEE, 2012), pp. 1–4.
- <sup>57</sup>T. Fushiki, "Estimation of prediction error by using *K*-fold cross-validation," Stat. Comput. **21**, 137–146 (2011).
- <sup>58</sup>V. Cherkassky and Y. Ma, "Practical selection of SVM parameters and noise estimation for SVM regression," Neural Netw. 17, 113–126 (2004).
- <sup>59</sup> A. N. Pisarchik, A. V. Andreev, S. A. Kurkin, D. Stoyanov, A. A. Badarin, R. Paunova, and A. E. Hramov, "Topology switching during window thresholding fMRI-based functional networks of patients with major depressive disorder: Consensus network approach," Chaos 33, 093122 (2023).
- <sup>60</sup> V. S. Khorev, S. A. Kurkin, G. Zlateva, R. Paunova, S. Kandilarova, M. Maes, D. Stoyanov, and A. E. Hramov, "Disruptions in segregation mechanisms in fMRI-based brain functional network predict the major depressive disorder condition," Chaos, Solitons Fractals 188, 115566 (2024).
- <sup>61</sup>S. A. Kurkin *et al.*, "Beyond pairwise interactions: Higher-order Q-analysis of fMRI-based brain functional networks in patients with major depressive disorder," IEEE Access **12**, 197168–197186 (2024).
- <sup>62</sup>Y. Benjamini and Y. Hochberg, "Controlling the false discovery rate: A practical and powerful approach to multiple testing," J. R. Stat. Soc. Ser. B 57, 289–300 (1995).
- <sup>63</sup>C. Lord and R. Luyster, "Early diagnosis of children with autism spectrum disorders," Clin. Neurosci. Res. **6**, 189–194 (2006).
- <sup>64</sup>N. Gabbay-Dizdar, M. Ilan, G. Meiri, M. Faroy, A. Michaelovski, H. Flusser, I. Menashe, J. Koller, D. A. Zachor, and I. Dinstein, "Early diagnosis of autism in the community is associated with marked improvement in social symptoms within 1–2 years," Autism 26, 1353–1363 (2022).
- <sup>65</sup>P. McCarty and R. E. Frye, "Early detection and diagnosis of autism spectrum disorder: Why is it so difficult?" in *Seminars in Pediatric Neurology* (Elsevier, 2020), Vol. 35, p. 100831.

- <sup>66</sup>N. Alotaibi and K. Maharatna, "Classification of autism spectrum disorder from EEG-based functional brain connectivity analysis," Neural Comput. 33, 1914–1941 (2021).
- <sup>67</sup>D. Haputhanthri, G. Brihadiswaran, S. Gunathilaka, D. Meedeniya, Y. Jayawardena, S. Jayarathna, and M. Jaime, "An EEG based channel optimized classification approach for autism spectrum disorder," in *2019 Moratuwa Engineering Research Conference (MERCon)* (IEEE, 2019), pp. 123–128.
- <sup>68</sup> J. Kang, X. Han, J. Song, Z. Niu, and X. Li, "The identification of children with autism spectrum disorder by SVM approach on EEG and eye-tracking data," Comput. Biol. Med. 120, 103722 (2020).
- <sup>69</sup>M. N. A. Tawhid, S. Siuly, H. Wang, F. Whittaker, K. Wang, and Y. Zhang, "A spectrogram image based intelligent technique for automatic detection of autism spectrum disorder from EEG," PLoS One 16, e0253094 (2021).
- <sup>70</sup>M. Arora, C. S. Jain, L. B. Baru, K. Dadi et al., "HyperGALE: ASD classification via hypergraph gated attention with learnable hyperedges," in 2024 International Joint Conference on Neural Networks (IJCNN) (IEEE, 2024), pp. 1–8.
- pp. 1–8. <sup>71</sup>G. Shen and W. Zeng, "Hypergraph label contrastive learning for autism spectrum disorder classification," in 2024 5th International Conference on Computer Vision, Image and Deep Learning (CVIDL) (IEEE, 2024), pp. 768–773.
- <sup>72</sup>J. Yang, F. Wang, Z. Li, Z. Yang, X. Dong, and Q. Han, "Constructing high-order functional networks based on hypergraph for diagnosis of autism spectrum disorders," Front. Neurosci. 17, 1257982 (2023).
- <sup>73</sup> A. N. Pisarchik, N. Peña Serrano, W. Escalante Puente de la Vega, and R. Jaimes-Reátegui, "Hypergraph analysis of functional brain connectivity during figurative attention," Appl. Sci. 15, 3833 (2025).